ChemComm

Crystalline to Amorphous Transformation in Solid-Solution Alloy Nanoparticles Induced by Boron Doping

Journal:	*ChemComm*
Manuscript ID	CC-COM-08-2020-005418.R1
Article Type:	Communication

Journal Name

COMMUNICATION

Crystalline to Amorphous Transformation in Solid-Solution Alloy Nanoparticles Induced by Boron Doping

Keigo Kobayashi,[a] Kohei Kusada,[a] Dongshuang Wu,[a] Naoki Ogiwara,[a,†] Hirokazu Kobayashi,*[,a,b] Mitsutaka Haruta,[c] Hiroki Kurata,[c] Satoshi Hiroi,[d,e] Okkyun Seo,[d,f] Chulho Song,[f] Yanna Chen,[d,f] Jae Myung Kim,[f] Akhil Tayal,[f] Osami Sakata,[d,e,f,g] Koji Ohara,[e] Tetsuo Honma [e] and Hiroshi Kitagawa *[,a,h,i]

Received 00th January 20xx,
Accepted 00th January 20xx

DOI: 10.1039/x0xx00000x

www.rsc.org/

We synthesized a palladium–ruthenium–boron (Pd–Ru–B) solid-solution ternary alloy. Elemental mappings confirmed successful alloying of B with Pd–Ru body without changing the particle sizes, demonstrating the first discovery of this ternery alloy. Pair distribution function analysis revealed a drastic decrease in atomic correlation in Pd–Ru nanoparticles by B doping. This result gives the first example of structural transformation from crystalline to amorphous in solid-solution alloy nanoparticles induced by the doping of light elements.

Crystallinity is one of the important factors that reflect the nature of materials. Compared with crystalline materials, amorphous solids or glass exhibit unique properties[1] such as high mechanical strength, soft magnetism, and high corrosion resistance because of their low crystallinities.

The formation criteria of bulk metallic glasses (BMGs) have often been described by Inoue's three empirical rules.[2] BMGs mainly consist of three or more elements which have large (> 12%) mismatching of atomic sizes, and their mixing enthalpy is largely negative among major constituent elements. To fulfil these conditions, light elements such as B, C, Si and P have been frequently used as alloying elements with transition metals and/or rare-earth metals.

Recently, amorphous metal nanoparticles (NPs), including light elements[3–6] have attracted tremendous attention as functional materials. For instance, Fe–Zr–B amorphous NPs[7] afforded magnetic fluid with superior thermomagnetic properties to magnetic fluid based on crystalline Fe_3O_4. Pd–Ni–P amorphous NPs[8] exhibited a higher catalytic performance compared with Pd, Pd–Ni, and even Pd–Ni–P crystalline counterparts. Among light elements, B is often used as a constituent element of amorphous metal NPs. B atoms can readily be produced by the decomposition of the borohydride anion (BH_4^-), which works as a reducing agent to transition metal cations, providing metal NPs. Up to now, many trials for the synthesis of amorphous alloy NPs consisting of B and transition metals such as Fe,[9–12] Co,[13–15] Ni[16–20] or Ru[12,21] have been performed. However, because of the lack of detailed characterization, the existence or concentration of B atoms in their NPs is still unclear.

Here, we report Pd–Ru–B alloy NPs wherein we found a unique structural change from crystalline to amorphous by B external doping. Nanosized crystalline–amorphous structural change induced by B external doping has been observed only in Fe–B amorphous NPs prepared from α-FeOOH crystalline NPs.[22,23] However, there have been no reports regarding solid-solution alloy NPs. Several kinds of characterizations confirmed the alloying of B with transition metals and the significant decrease of interatomic correlation after B doping. This work may propose a new synthetic method to fabricate amorphous metal NPs containing B.

[a] Division of Chemistry, Graduate School of Science, Kyoto University, Kitashirakawa-Oiwakecho, Sakyo-ku, Kyoto 606-8502, Japan
[b] Precursory Research for Embryonic Science and Technology (PRESTO), Japan Science and Technology Agency (JST), 4-1-8 Honcho, Kawaguchi, Saitama 332-0012, Japan
[c] Institute for Chemical Research, Kyoto University, Gokasho, Uji, Kyoto 611-0011, Japan
[d] Synchrotron X-ray Group, Research Center for Advanced Measurement and Characterization, National Institute for Materials Science (NIMS), 1-1-1 Kouto, Sayo-cho, Sayo-gun Hyogo 679-5148, Japan
[e] Japan Synchrotron Radiation Research Institute, 1-1-1 Kouto, Sayo-cho, Sayo-gun, Hyogo 679-5198, Japan
[f] Synchrotron X-ray Station at SPring-8, NIMS, 1-1-1 Kouto, Sayo-gun, Hyogo 679-5148, Japan
[g] Department of Materials Science and Engineering, School of Materials and Chemical Technology, Tokyo Institute of Technology, Yokohama 226-8502, Japan
[h] INAMORI Frontier Research Center, Kyushu University, Motooka 744, Nishi-ku, Fukuoka 819-0395, Japan
[i] Institute for Integrated Cell-Material Sciences (iCeMS), Kyoto University, Yoshida, Sakyo-ku, Kyoto 606-8501, Japan
† Current address: Department of Basic Science, School of Arts and Sciences, The University of Tokyo, 3-8-1 Komaba, Meguro-ku, Tokyo 153-8902, Japan.
Electronic Supplementary Information (ESI) available. See DOI: 10.1039/x0xx00000x

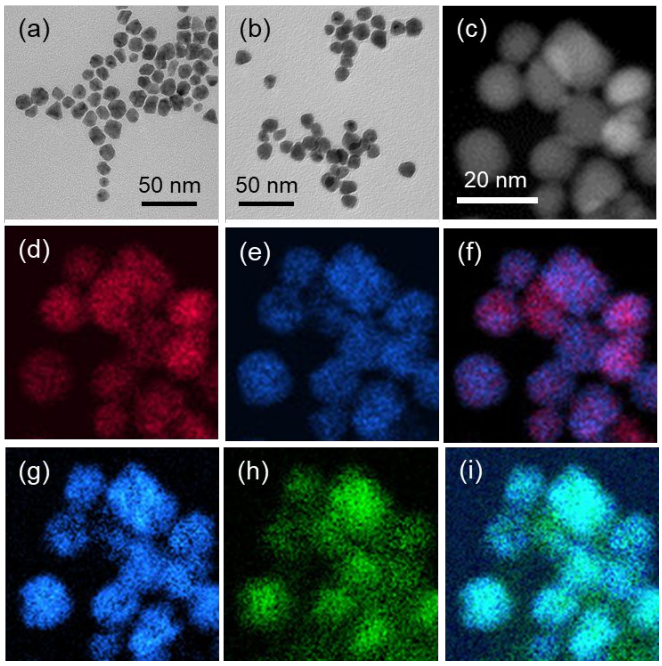

Fig. 1 Low-magnification TEM images of (a) Pd–Ru and (b) Pd–Ru–B NPs, respectively. (c) HAADF-STEM image, EDS mappings of (d) Pd-*L*, (e) Ru-*L*, (f) overlay of Pd and Ru, EELS mappings of (g) Ru-*L*, (h) B-*K* and (i) overlay of Ru and B of Pd–Ru–B NPs.

The amorphous Pd–Ru–B NPs were prepared by two-step synthesis. First, we prepared poly-(*N*-vinyl-2-pyrrolidone) (PVP)-coated Pd–Ru NPs by a previously reported procedure.[24] The Pd–Ru–B NPs were obtained by adding BH_3–THF in the presence of the prepared Pd–Ru NPs at 80 ˚C under N_2 flow. After continuous stirring for 2 days, the products were retrieved by centrifugation.

From transmission electron microscopy (TEM) images, the mean diameters of Pd–Ru and Pd–Ru–B NPs were estimated to be 12.9 ± 1.8 and 12.9 ± 1.9 nm, respectively (see Fig. 1(a), (b) and Fig. S1 in Supplementary Information). The mean diameter was maintained before and after the introduction of B into Pd–Ru NPs.

To investigate the distribution of B atoms in Pd–Ru NPs, we combined the energy-dispersive X-ray spectroscopy (EDS) and electron-energy loss spectroscopy (EELS) analyses of Pd–Ru–B NPs. Fig. 1(c)–(e) show a high-angle annular dark-field (HAADF)-scanning TEM (STEM) image and EDS maps of Pd-*L* and Ru-*L* for Pd–Ru–B NPs, respectively. Fig. 1(f) shows an overlay map of Pd and Ru elements. The overlay map revealed that the Pd–Ru solid-solution structure was maintained after B doping. From EDS analysis, the distribution of B atoms in Pd–Ru–B NPs could not be precisely determined because the B-*K* signal overlaps with the C-*K* signal originating from PVP. Therefore, we performed EELS measurement (Fig. 1(g)–(i)). An overlay map of Ru-*L* and B-*K* revealed that Ru and B atoms were randomly and homogeneously mixed. The combination of EDS and EELS maps demonstrated the formation of Pd–Ru–B solid-solution ternary alloy NPs, in which three elements were randomly and homogeneously distributed in each NP. The atomic ratios of Pd, Ru and B were estimated to be approximately 1:1:1 by X-ray fluorescence spectroscopy and EELS (Fig. S2 in Supplementary Information).

To investigate the crystal structure of Pd–Ru–B NPs, we measured X-ray diffraction (XRD) at beamline BL04B2 in SPring-8. Fig. 2(a) shows the XRD patterns of the Pd–Ru and Pd–Ru–B NPs. The XRD pattern of Pd–Ru NPs revealed that Pd–Ru NPs are crystalline and have mixture phases of face-centred cubic (fcc) and hexagonal close-packed (hcp) structures (see Fig. S3), which is consistent with the previous report.[24] The existence of the hcp component was confirmed from the Rietveld refinement of Pd–Ru NPs. From the Rietveld refinement of the diffraction pattern for $Pd_{0.5}Ru_{0.5}$ NPs, the lattice constants for the two components were found to be a = 3.859(1) Å for the fcc lattice and a = 2.732(2) Å and c = 4.386(8) Å for the hcp lattice. In contrast, the diffraction peaks of Pd–Ru–B NPs were much broader than those of Pd–Ru NPs. The diffraction pattern of Pd–Ru–B NPs suggests that the introduction of B atoms into Pd–Ru NPs induces a highly disordered structure.

As a structural characterization of poorly crystalline materials including amorphous[25] and liquid materials,[26,27] pair distribution function (PDF) analysis based on high-energy XRD (HEXRD) has been a powerful tool to determine the local structures. Recently, PDF analysis has also been applied to nanomaterials such as bimetallic NPs[28] and quantum dots.[29] Here, we provide the structural information of ternary alloy NPs by PDF analysis. Fig. S4(a) and S4(b) show the X-ray total structure factor $S(Q)$, which is a diffraction intensity normalized

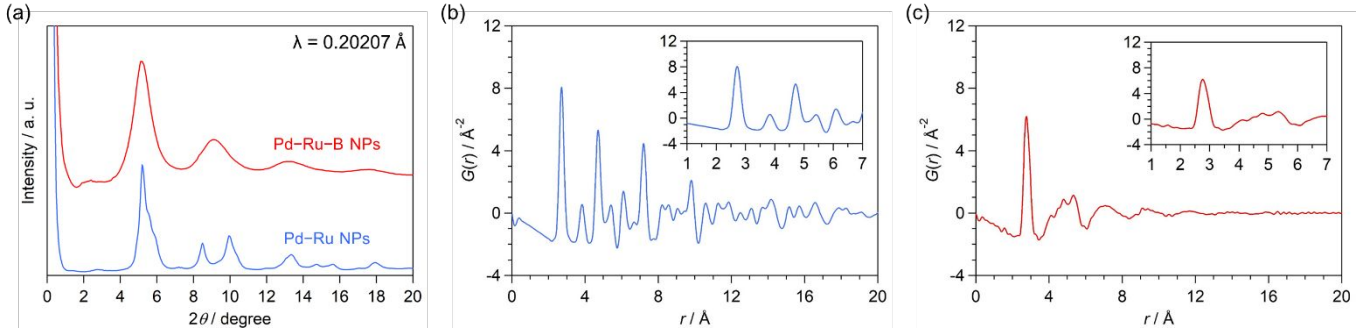

Fig. 2 (a) HEXRD intensity $I(Q)$, total pair distribution $G(r)$ obtained by Fourier transform of the $S(Q)$ of (b) Pd–Ru and (c) Pd–Ru–B NPs. The insets of (b) and (c) are the magnified images at the range of r between 1 Å and 7 Å. Each spectrum of Pd–Ru–B NPs and Pd–Ru NPs was measured at 233 K and at RT, respectively.

by the number of electrons of Pd–Ru and Pd–Ru–B NPs, respectively. Although the oscillation line width of Pd–Ru–B NPs is broader than that of Pd–Ru NPs because of the highly disordered structure, the oscillation of $S(Q)$[30] of Pd–Ru–B NPs is observable up to a high-Q region. This result suggests that the interatomic correlation still exists in amorphous Pd–Ru–B NPs. Then, the obtained total PDF $G(r)$ by Fourier transform of the $S(Q)$ of each sample is represented in Fig. 2(b) and 2(c). The existence of the hcp component can be also inferred from the spectra of $S(Q)$ and $G(r)$ of Pd–Ru NPs (Figs. S5 and S6). As shown in Fig. 2(b) and 2(c), the first nearest-neighbour peak of Pd–Ru–B NPs was observed as well as that of Pd–Ru NPs. The first nearest-neighbour peaks were located at r = 2.76 Å in Pd–Ru–B NPs, whereas those of Pd–Ru NPs were at r = 2.71 Å. This result indicates that the doping of B atoms slightly expands the nearest-neighbour interatomic distance between metal atoms in amorphous Pd–Ru–B NPs. In contrast, the peaks after the second nearest-neighbour position of Pd–Ru–B NPs were blurred, compared with those of Pd–Ru NPs. Considering that the oscillation of the $G(r)$ spectrum of Pd–Ru–B NPs was observed up to around 16 Å, a short-range atomic order of 1.6 nm likely exists in amorphous Pd–Ru–B NPs with a mean diameter of 12.9 nm.

To further confirm the highly disordered structure of Pd–Ru–B NPs, synchrotron X-ray absorption spectroscopy was performed at beamline BL14B2 of SPring-8. Fig. 3 shows extended X-ray absorption fine structure (EXAFS) oscillation of the Pd–Ru and Pd–Ru–B NPs measured at room temperature. The results show that the oscillation amplitude of Pd–Ru–B NPs markedly decreased compared with that of Pd–Ru NPs. The decrease in oscillation amplitude originates from an increase of the Debye–Waller factor, supporting the formation of the amorphous structure of Pd–Ru–B NPs.

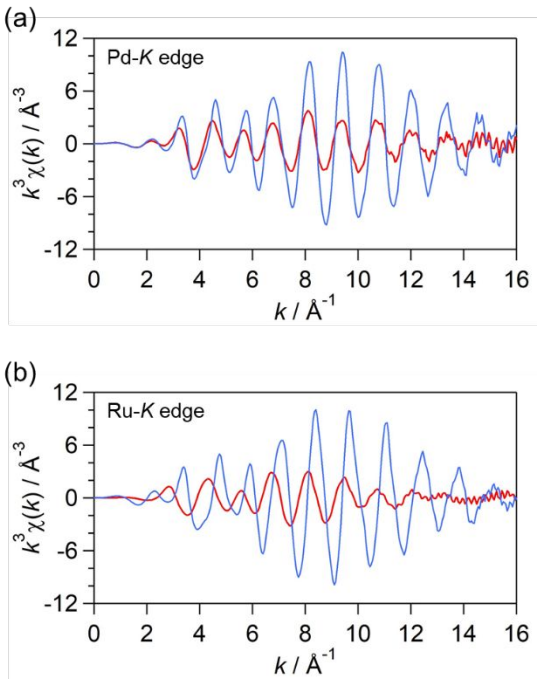

Fig. 3 EXAFS oscillation spectra of (a) Pd-*K* and (b) Ru-*K* edges. Red and blue curve corresponds to Pd–Ru–B and Pd–Ru NPs, respectively.

These results are consistent with the selected area electron diffraction (SAED). Fig. S7(a) shows a TEM image of Pd–Ru–B NPs, and S7(b) shows an SAED pattern of the corresponding region. It displays the typical halo-ring character originating from an amorphous structure. However, some diffraction spots observed in Fig. S7(b) suggest that B atoms of Pd–Ru–B NPs were partially released to change from an amorphous Pd–Ru–B structure to a crystalline Pd–Ru structure. The similar trend was observed in HAADF-STEM image and corresponding fast Fourier transforms shown in Fig. S8.

Fig. 4 shows that the Pd–Ru–B amorphous structure gradually transforms into the Pd–Ru crystalline structure even

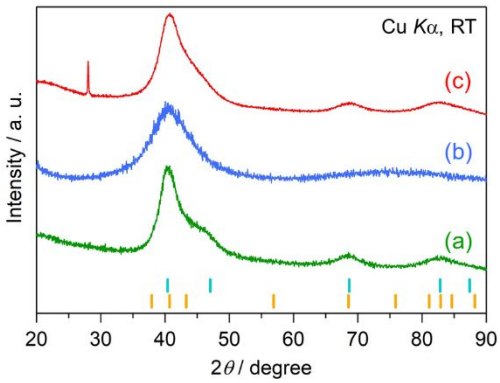

Fig. 4 PXRD patterns of (a) Pd–Ru NPs ($Pd_{53}Ru_{47}$), (b) Pd–Ru–B NPs and (c) Pd–Ru–B NPs after 3 years under air. Markers at the bottom show simulated peak positions of fcc (light blue) and hcp (orange) component, respectively.

under ambient conditions. It partially changed to a Pd–Ru structure after 3 years under air. A sharp peak is observed around $2\theta \sim 28^\circ$ in Fig. 4(c) that might be attributed to B_2O_3.[31] This decomposition can be considered to result from a weak chemical interaction between B atoms and Pd or Ru atoms, suggested by an insensitivity of X-ray absorption near-edge structure spectra of Pd-*K* or Ru-*K* edges against B introduction (Fig. S9). The white lines of Pd–Ru and Pd–Ru–B NPs were located at almost the same energy value in both Pd-*K* and Ru-*K* edges. There should be a weak, or almost no electronic interaction between B and Pd or Ru. B atoms can easily escape from the ternary alloy and segregate into Pd–Ru NPs and B_2O_3. Thus far, there exist few theories[32,33] that discuss the formation mechanism of amorphous alloy NPs. Future development of experimental and theoretical investigation is needed to clarify the amorphous formability of NPs.

In summary, we describe the formation of amorphous Pd–Ru–B NPs from crystalline Pd–Ru NPs. From the combined measurement of EDS and EELS, the distribution of each element was investigated. PDF analysis taken from the HEXRD pattern revealed the absence of long-range order but the elongation of the first nearest-neighbour distance. This work is the first to report that Pd–Ru nanosystem exhibits a crystalline–amorphous transformation by external B doping.

This research was supported by the ACCEL program, Japan Science and Technology Agency (JST), JPMJAC1501 and Grant-in-Aid for Specially Promoted Research 20H05623. STEM observations were performed as part of a programme conducted by the Advanced Characterization Nanotechnology

Platform sponsored by the Ministry of Education, Culture, Sports, Science and Technology (MEXT), Japan. Synchrotron XRD and XAFS measurements were supported by the Japan Synchrotron Radiation Research Institute (JASRI) (Proposal Nos. 2018A1351 and 2018A1753). We thank Mr. Yamamoto, Mr. Toriyama and Prof. Matsumura at Kyushu University for kind assistance of HAADF-STEM observation and fruitful discussions.

H. Kobayashi and H. Kitagawa designed this study. K. Kobayashi performed the experiments. K. Kusada and D. Wu assisted with the synthesis. M. Haruta and H. Kurata conducted the HAADF-STEM observation, EDS or EELS mapping and SAED measurement. S. Hiroi, O. Seo, C. Song, Y. Chen, J. M. Kim, A. Tayal, O. Sakata and K. Ohara assisted with the synchrotron HEXRD measurements. N. Ogiwara and T. Honma assisted with the XAFS measurements. K. Kobayashi, H. Kobayashi, K. Kusada and H. Kitagawa co-drafted the manuscript. All authors contributed to the manuscript.

Conflicts of interest

There are no conflicts to declare.

Notes and references

1 W. H. Wang, C. Dong and C. H. Shek, *Mater. Sci. Eng. R Rep.*, 2004, **44**, 45–89.
2 A. Inoue, *Acta Mater.*, 2000, **48**, 279–306.
3 T. Wang, X. Bian, C. Yang, S. Zhao and M. Yu, *Appl. Surf. Sci.*, 2017, **399**, 663–669.
4 W.-J. Wang, J.-H. Shen and Y.-W. Chen, *Ind. Eng. Chem. Res.*, 2006, **45**, 8860–8865.
5 M. Ren, C. Li, J. Chen, M. Wei and S. Shi, *Catal. Sci. Technol.*, 2014, **4**, 1920–1924.
6 M. Zhao, Y. Ji, M. Wang, N. Zhong, Z. Kang, N. Asao, W.-J. Jiang and Q. Chen, *ACS Appl. Mater. Interfaces*, 2017, **9**, 34804–34811.
7 J. Wang, M. Fan, X. Bian, M. Yu, T. Wang, S. Liu, Y. Yang, Y. Tian and R. Guan, *J. Magn. Magn. Mater.*, 2018, **465**, 480–488.
8 M. Zhao, Y. Ji and N. Zhong, *Int. J. Electrochem. Sci.*, 2016, **11**, 10488–10497.
9 Z. J. Yan and D. S. Xue, *J. Mater. Sci.*, 2008, **43**, 771–774.
10 V. G. de Resende, E. De Grave, G. M. da Costa and J. Janssens, *J. Alloys Compd.*, 2007, **440**, 248–253.
11 Y. Pei, J. Wang, Q. Fu, P. Guo, M. Qiao, S. Yan and K. Fan, *New J. Chem.*, 2005, **29**, 992–994.
12 S. Liu, Z. Liu, S. Zhao, Y. Wu, Z. Wang and P. Yuan, *J. Nat. Gas Chem.*, 2006, **15**, 319–326.
13 Z.-J. Liu, Z. Xu, Z.-Y. Yuan, W. Chen, W. Zhou and L.-M. Peng, *Mater. Lett.*, 2003, **57**, 1339–1344.
14 J.-H. Shen and Y.-W. Chen, *J. Mol. Catal. Chem.*, 2007, **273**, 265–276.
15 M. Mo, M. Zheng, J. Tang, Q. Lu and Y. Xun, *J. Mater. Sci.*, 2014, **49**, 877–885.
16 X. Chen, Z. Lou, S. Xie, M. Qiao, S. Yan, Y. Zhu, K. Fan and H. He, *Chem. Lett.*, 2006, **35**, 390–391.
17 C.-Y. Hu, F.-Y. Li, R.-B. Zhang, X.-N. Liao and L. Hua, *J. Chin. Chem. Soc.*, 2007, **54**, 559–562.
18 W. Zhang, X. Zhang, Y. Tan, J. Wu, Y. Gao, B. Tang and Y. Wang, *New J. Chem.*, 2014, **38**, 4666–4669.
19 G. Xie, W. Sun and W. Li, *Catal. Commun.*, 2008, **10**, 333–335.
20 W. Wang, P. Liu, K. Wu, K. Zhang, L. Li, Z. Qiao and Y. Yang, *New J. Chem.*, 2015, **39**, 813–816.
21 S. Xu, F. Li and R. Wei, *Carbon*, 2005, **43**, 861–864.
22 V. G. de Resende, E. De Grave, G. M. da Costa and J. Janssens, *J. Alloys Compd.*, 2007, **440**, 248–253.
23 Z. Enlei, L. Ning, Z. Bengui, X. Yingpeng and W. Guosheng, *J. Nanosci. Nanotechnol.*, 2017, **17**, 2140–2144.
24 K. Kusada, H. Kobayashi, R. Ikeda, Y. Kubota, M. Takata, S. Toh, T. Yamamoto, S. Matsumura, N. Sumi, K. Sato, K. Nagaoka and H. Kitagawa, *J. Am. Chem. Soc.*, 2014, **136**, 1864–1871.
25 J. Antonowicz, D. V. Louzguine-Luzgin, A. R. Yavari, K. Georgarakis, M. Stoica, G. Vaughan, E. Matsubara and A. Inoue, *J. Alloys Compd.*, 2009, **471**, 70–73.
26 A. Posada-Amarillas and I. L. Garzón, *Phys. Rev. B*, 1996, **53**, 8363–8368.
27 G. W. Neilson, A. K. Adya and S. Ansell, *Annu. Rep. Sect. C Phys. Chem.*, 2002, **98**, 273–322.
28 V. Petkov, B. N. Wanjala, R. Loukrakpam, J. Luo, L. Yang, C.-J. Zhong and S. Shastri, *Nano Lett.*, 2012, **12**, 4289–4299.
29 V. Petkov, M. Gateshki, J. Choi, E. G. Gillan and Y. Ren, *J. Mater. Chem.*, 2005, **15**, 4654–4659.
30 L. S. R. Kumara, O. Sakata, S. Kohara, A. Yang, C. Song, K. Kusada, H. Kobayashi and H. Kitagawa, *Phys. Chem. Chem. Phys.*, 2016, **18**, 30622–30629.
31 J. Jiang, B. J. Senkowicz, D. C. Larbalestier and E. E. Hellstrom, *Supercond. Sci. Technol.*, 2006, **19**, L33–L36.
32 S. Xiao, X. Li, H. Deng, L. Deng and W. Hu, *Phys. Chem. Chem. Phys.*, 2015, **17**, 6511–6522.
33 A. Umantsev, *Acta Mater.*, 2013, **61**, 1106–1117.